Chapter 19
Parameter Identification of Nonlinear Viscoelastic Material Model Using Finite Element-Based Inverse Analysis

Salah U. Hamim and Raman P. Singh

Abstract This study focuses on identifying the parameters of a nonlinear viscoelastic model from Berkovich nanoindentation experiment of an epoxy polymer using finite element-based inverse analysis approach. Instead of traditional approach of online optimization of model parameters, where finite element computation is placed inside of the optimization algorithm, this study utilizes a surrogate or meta-modeling approach. The surrogate model, which is based on Proper Orthogonal Decomposition (POD) and Radial Basis Function (RBF), is trained with finite element load–displacement data obtained by varying the different model parameters in a parameter space. Once trained POD–RBF based surrogate model is used to approximate the nanoindentation simulation data inside a multi-objective Genetic Algorithm. Current efforts are focused to validate identified parameter set of nonlinear viscoelastic model for different experimental conditions (e.g. maximum load, loading/unloading rate).

Keywords Taguchi orthogonal array • Nonlinear viscoelastic model • Finite element analysis • Radial basis function • Proper orthogonal decomposition

19.1 Introduction

Polymer materials have found applications in a wide variety of industries in the last few decades e.g. automotive, aerospace, packaging, and microelectronics. Unlike most materials polymer exhibit time-dependent mechanical response. Due to the inherent viscoelastic or viscoplastic behavior, understanding long-term mechanical response of these materials has been a challenge.

In addition to that, these materials are often used in micro- or nano-scale applications, e.g. thin films. Conventional testing methods, which can only provide the macro-scale mechanical behavior, are not suitable in characterizing nano- or micro-scale behavior of these materials [1, 2]. If a material system is non-homogeneous, such as ultraviolet irradiated polymer surface or nanofiller reinforced polymer, macro-scale test data fails to reflect the localized changes in a material [3]. In these situations nanoindentation or depth sensing indentation (DSI) can provide nano-scale mechanical behavior due to its high spatial resolution [4].

However, relating nanoindentation load–displacement data to mechanical properties requires suitable analytical or numerical methods [5, 6]. For materials exhibiting simple elastic or elastoplastic behavior, use of nanoindentation has been widely reported [7–10]. On the contrary, for materials exhibiting time-dependent mechanical behavior, the application of nanoindentation is still a challenge [11].

In this study, model parameters of a nonlinear viscoelastic model has been identified using finite element-based inverse analysis and a global optimization technique known as genetic algorithm (GA). Calibrating a complex mechanical constitutive relationship with the help of genetic algorithm is computationally expensive when finite element analysis is placed within the optimization algorithm. To circumvent this issue, a surrogate model trained with finite element data is used within the optimization loop. The surrogate model has been created using Proper Orthogonal Decomposition (POD) and Radial Basis Function (RBF) technique. The number of training points for the surrogate model has been reduced by utilizing the sensitivity of individual model parameters.

S.U. Hamim (✉) • R.P. Singh
School of Mechanical and Aerospace Engineering, Oklahoma State University, Stillwater, OK 74075, USA
e-mail: raman.singh@okstate.edu

S. Quinn, X. Balandraud (eds.), *Residual Stress, Thermomechanics & Infrared Imaging, Hybrid Techniques and Inverse Problems, Volume 9*, Conference Proceedings of the Society for Experimental Mechanics Series, DOI 10.1007/978-3-319-42255-8_19

19.2 Experimental Details

19.2.1 Materials

An epoxy polymer, named EPON 862, was selected for carrying out nanoindentation experiments. EPON 862 is a diglycidyl ether of bisphenol F (DGEBF). The curing agent used for this resin system was a moderately reactive, low viscosity aliphatic amine curing agent, called Epikure 3274. Both of these chemicals were supplied by Miller-Stephenson Chemical Company, Inc., Dunbury, Connecticut.

Epoxy and hardener was mixed at 100:40 weight ratio and hand-mixed using a glass-rod for 5–10 min. The mixture was then degassed for around 10–20 min to remove any entrapped air bubbles. The mixture was then poured into an aluminum mold and cured at room temperature for 24 h and subsequently post-cured at 121 °C for 6 h. The final sample was cut from the prepared epoxy plate using a bandsaw. Sample surface preparation was carried out by polishing using standard metallographic techniques.

19.2.2 Nanoindentation

Nanoindentation experiments were conducted on an MTS Nanoindenter XP (Agilent Technologies, Santa Clara, CA, USA) using a load-controlled scheme with a Berkovich tip. The maximum load was set to be 1.0 mN for the experiments. A triangular loading profile was chosen with 30, 45, 60, and 240 s durations. The durations were kept constant for both the loading and unloading segments.

Before conducting the actual experiments the Berkovich tip was calibrated using a fused silica reference material. Also, the acceptable thermal drift rate was chosen to be 0.15 nm/s. After ensuring that the thermal drift rate was stable and below the target drift rate nanoindentation experiments were carried out.

19.2.3 Material Model

In this study, a spring–dashpot model developed by Marin and Pao [12] was used. In linear case this model is generally called four-parameter Burgers model [13] and it is formed by a serial connection of a Maxwell element to a Voigt element. For an increased relaxation spectrum, the viscoelastic response can be modeled by increasing the number of Voigt elements.

The nonlinear characteristic is introduced when the dashpot constants (m_s and m_t) take values other than unity. In the three-dimensional model, the total strains are calculated as the summation of the elastic (ε^e), transient creep (ε^t), and steady creep strains (ε^s) [14]. In this study, the nonlinear creep deformation is assumed to be incompressible. Under these assumptions, the three-dimensional nonlinearly viscoelastic law can be expressed as:

$$\varepsilon_{ij}^{e} = \frac{1+\nu}{E}\sigma_{ij} - \frac{\nu}{E}\sigma_{kk}\delta_{ij} \tag{19.1}$$

$$\dot{\varepsilon}_{ij}^{s} = C_s J_2^{m_s}(t) s_{ij}(t) \tag{19.2}$$

$$\dot{\varepsilon}_{ij}^{t} + \frac{\varepsilon_{ij}^{t}}{t_\varepsilon} = \frac{C_t}{t_\varepsilon} J_2^{m_t}(t) s_{ij}(t) \tag{19.3}$$

where E, ν are the Young's modulus and Poisson ratio, respectively; J_2 is the second invariant of the deviator stress tensor s; C_s, C_t, m_s, m_t, t_ε are the nonlinear material parameters. σ is the Cauchy stress tensor; i, j are the indices ranging among 1–3. δ_{ij} is the Kronecker delta which used in the context of summation convention with the well-known property $\delta_{ij} = 1$ when i = j and $\delta_{ij} = 0$ otherwise. Small deformations are assumed in the formulation. When more than one Voigt element is included in the model, the total strain components can be given as the sum of elastic, steady creep, and transient creep components for all Voigt elements,

$$\varepsilon_{ij} = \varepsilon_{ij}^{e} + \varepsilon_{ij}^{s} + \varepsilon_{ij}^{t} = \varepsilon_{ij}^{e} + \varepsilon_{ij}^{s} + \sum_{i=1}^{n} \varepsilon_{ij}^{t_i} \tag{19.4}$$

where n is the number of Voigt elements. Equations (19.2) and (19.3) can also be written in integral form:

$$\varepsilon_{ij}^{s} = C_s \int_0^t J_2^{m_s}(t') s_{ij}(t') dt' \tag{19.5}$$

$$\varepsilon_{ij}^{t} = \frac{C_t}{t_\varepsilon} e^{(-t/t_\varepsilon)} \int_0^t J_2^{m_t}(t') s_{ij}(t') e^{(-t'/t_\varepsilon)} dt' \tag{19.6}$$

An UMAT was developed in order to implement the nonlinear Burgers model. UMAT requires the tangent stiffness matrix of the material model for finite element calculations. For implementation of the nonlinear Burgers viscoelastic model, the UMAT required temporal discretization. This was done following the procedure implemented by Kucuk et al. [15, 16]. A simple, stable integration operator for these equations is the central difference operator:

$$\dot{f}_{\,t+\frac{1}{2}\Delta t} = \frac{\Delta f}{\Delta t}, f_{t+\frac{1}{2}\Delta t} = f_t + \frac{\Delta f}{2} \tag{19.7}$$

where f is a function, f_t is its value at the beginning of the increment, Δf is the change in the function over the increment, and Δt is the time increment.

Tangent stiffness matrix $\delta \Delta \sigma / \delta \Delta \varepsilon$ of the constitutive model, with $\Delta \sigma$ being the stress increments and $\Delta \varepsilon$ the strain increments, can be derived by applying central difference operator to the rate-dependent constitutive equations (Eqs. (19.1)–(19.3)). The compliance matrices obtained for these three equations are given below–

$$C = \begin{bmatrix} 1/E & -\nu/E & -\nu/E & 0 & 0 & 0 \\ & 1/E & -\nu/E & 0 & 0 & 0 \\ & & 1/E & 0 & 0 & 0 \\ & & & \frac{1+\nu}{E} & 0 & 0 \\ & & & & \frac{1+\nu}{E} & 0 \\ & & & & & \frac{1+\nu}{E} \end{bmatrix}_{symmetric} \tag{19.8}$$

$$C = \Delta t C_s J_2^{m_s}(t) \begin{bmatrix} 1/3 & 0 & 0 & 0 & 0 & 0 \\ & 1/3 & 0 & 0 & 0 & 0 \\ & & 1/3 & 0 & 0 & 0 \\ & & & 1/2 & 0 & 0 \\ & & & & 1/2 & 0 \\ & & & & & 1/2 \end{bmatrix}_{symmetric} \tag{19.9}$$

$$C = \frac{\Delta t}{2t_\varepsilon + \Delta t} C_t J_2^{m_t}(t) \begin{bmatrix} 2/3 & 0 & 0 & 0 & 0 & 0 \\ & 2/3 & 0 & 0 & 0 & 0 \\ & & 2/3 & 0 & 0 & 0 \\ & & & 1 & 0 & 0 \\ & & & & 1 & 0 \\ & & & & & 1 \end{bmatrix}_{symmetric} \tag{19.10}$$

From Eq. (19.4), the total compliance is now

$$\frac{\delta \Delta \varepsilon_{ij}}{\delta \Delta \sigma_{kl}} = \frac{\delta \Delta \varepsilon_{ij}^e}{\delta \Delta \sigma_{kl}} + \frac{\delta \Delta \varepsilon_{ij}^s}{\delta \Delta \sigma_{kl}} + \frac{\delta \Delta \varepsilon_{ij}^t}{\delta \Delta \sigma_{kl}} \tag{19.11}$$

By investigating the total compliance matrix, system tangent stiffness matrix (Jacobian matrix) $\frac{\delta \Delta \sigma_{ij}}{\delta \Delta \varepsilon_{kl}}$ can be obtained from Eq. (19.11). It should be noted that the Jacobian matrix in Eq. (19.11) accounts only for the elastic deformation and creep deformation caused by load or stress increment. The rest of the creep strain is developed over the time period during the time increment and controlled by the applied stress. An artificial stress increment is introduced to include this creep strain in the system equation. This part of creep strain can be extracted as

$$\Delta \varepsilon' = \Delta t C_t J_2^{m_t}(t) s_{ij}(t) + \frac{1}{2t_\varepsilon + \Delta t} (2\Delta t C_t J_2^{m_t}(t) s_{ij}(t) - 2\Delta t \varepsilon^t) \tag{19.12}$$

A stress increment $\Delta \sigma' = C \Delta \varepsilon'$ is then added into the system equation to account for the creep strain in Eq. (19.12), with C being the Jacobian stiffness matrix calculated from Eq. (19.11).

19.2.4 Finite Element Modeling

The 3D finite element model of nanoindentation experiment was constructed using commercial finite element package ABAQUS (Dassault Systemes, Providence, RI). The Berkovich indenter was modeled as discrete rigid body, while the sample was modeled as deformable body.

To ensure accuracy of the simulation results, the sample was modeled with finer mesh near the contact area, where the stress and strain generated was much higher. The contact between the indenter and the sample was defined as surface-to-surface contact, where the indenter was designated as *master surface* and the sample was as designated as *slave surface*. The contact was assumed to have sliding friction with a friction coefficient of 0.25. The element types for the sample was chosen from the eight-node brick element family (C3D8). Material behavior of the sample was defined in the model using a subroutine (UMAT). Figure 19.1 shows the schematic of the finite element nanoindentation experiment model.

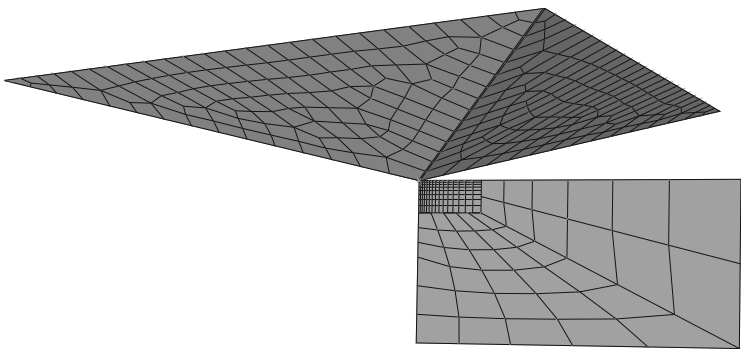

Fig. 19.1 Schematic of finite element model of Berkovich nanoindentation

Table 19.1 Levels of nonlinear Burgers model parameters

Parameters	Level 1	Level 2	Level 3
E	3	3.25	3.5
C_s	0.02	0.06	0.1
m_s	0.15	0.25	0.35
C_t	0.15	0.25	0.35
m_t	0.2	0.5	0.8
t_ε	0.1	0.25	0.4

19.2.5 Design of Experiments for Sensitivity Analysis

Before generating finite element simulation data by varying the model parameters, a sensitivity study of the parameters was conducted. This information helped to reduce the number of finite element simulation that was used to train a POD–RBF based surrogate model [17].

The nonlinear Burgers model that was chosen to represent the behavior of the epoxy has seven independent parameters. These parameters are E, ν, C_s, m_s, C_t, m_t, and t_ε. It is already known that a nanoindentation load–displacement response is not highly influenced by Poisson's ratio, ν [18–20]. Therefore, in order to keep the number of independent parameters to a minimum, ν was given a constant value of 0.34, and was not included in the sensitivity analysis scheme.

Sensitivity analysis was carried out using Analysis of Variance (ANOVA) technique. The data required for ANOVA was generated using the Taguchi Design of Experiments (DOE) method. In this study, the six nonlinear model parameters were varied in three equidistant levels. A statistical software, Minitab (Minitab Inc., State College, PA, USA) was used to design the experiments. For six parameters, where each parameters were varied in three levels, Taguchi L_{27} orthogonal array design was appropriate. Table 19.1 shows the levels of the six individual parameters of the nonlinear Burgers model. The experimental design required a total of 27 individual computer experiments. In these 27 experiments, except for material model parameters every other parameters (e.g. load, loading–unloading time, boundary conditions) were kept same.

Each of these 27 computer simulations resulted in data in terms of indenter displacement. The resulting value of error function, δ was calculated using the Eq. (19.13). This was then utilized in ANOVA to determine the effect of each parameters on the error function.

$$\delta = \frac{1}{n} \sum \left[\left(h^i_{exp} - h^i_{sim} \right)^2 \right] \tag{19.13}$$

In Eq. (19.13), $i = 1, 2, 3, \ldots, n$, and n is the number of data points in a single nanoindentation simulation or experiment.

19.2.6 POD–RBF Surrogate Model

The POD theory, also known as PCA, was developed to approximate a function over some domain of interest based on the known relationships between the input and the output [21–23]. This study followed the POD–RBF procedure outlined by Buljak [24] and Rogers et al. [25]. POD–RBF method requires creating snapshots (input–output relationships of the system) from which the surrogate model could be established. Each of the data that provides a one-to-one relationship between the input and the output is called a snapshot. The more snapshots or training data points that could be utilized to generate the surrogate model the better the approximation becomes.

However, the computational burden associated with generating large number of snapshots becomes the limiting factor in obtaining very high-fidelity predictions from the surrogate model. Sensitivity analysis could be utilized to reduce the number of snapshots without sacrificing approximation error [17]. Hence, in this study, a similar approach was adopted to reduce the computation burden of training the surrogate model for nonlinear Burgers model.

Once the appropriate number of levels for different parameters were selected using information from sensitivity analysis, a full factorial approach was taken to generate the input parameter sets. These parameter sets were combined to produce the input matrix, **P**. Finite element simulation experiments were carried out for every individual parameter sets and their corresponding indenter displacement data was assimilated in the snapshot matrix, **U**, which can be defined as–

$$U = \begin{bmatrix} u_1^1 & u_1^2 & \cdots & u_1^M \\ u_2^1 & u_2^2 & \cdots & u_2^M \\ \vdots & \vdots & \vdots & \vdots \\ u_N^1 & u_N^2 & \cdots & u_N^M \end{bmatrix} \tag{19.14}$$

In this study, four different experimental conditions were utilized for which the training data would be generated. In these experimental conditions, the maximum load was kept constant at 1 mN, while the strain rate was varied from 1/30 s^{-1} to 1/240 s^{-1}. One surrogate model was created for each of those experimental conditions using finite element data. The approximations from each surrogate model was compared against their own experimental indenter displacement data to form the objective or error function.

A Multiquadratic RBF was chosen for this study. Hamim and Singh reported that the value of the shape parameter (c_j) did not influence the POD–MQ RBF surrogate model's performance significantly [17]. So, for this study it was chosen 0.5.

19.2.7 Genetic Algorithm

A multi-objective genetic algorithm-based optimization procedure was used to identify the parameters of the nonlinear Burgers model. The procedure was implemented using MATLAB's (Mathworks Inc., Natick, MA, USA) global optimization toolbox.

An initial population of 200 was randomly created with a uniform distribution (*Double vector* population type). Scores of the first and all subsequent generations were determined by evaluating the fitness function that was submitted to the program via MATLAB script. *Selection* of the worthy candidates for being the next generation parent were carried out via tournament of size 2. Eighty percent of the next generation population was produced via *crossover*, while the remainder of the was created through *mutation*. Gaussian mutation was selected, where a random number from a Gaussian distribution centered on zero was added to each vector entry of an individual. *Scale* and *Shrink* parameters were set to 1 for this study.

In this study, the crossover function was chosen to be *intermediate*. Ratio = 1 was used for creating next generation children. Forward migration direction was chosen. This meant individuals from n^{th} subpopulation would replace individuals from $(n+1)^{th}$ subpopulation and so on. The migration fraction and interval were chosen to be 0.2 and 20, respectively. Total number of generations for the optimization algorithm was chosen to 100× number of parameters, i.e. $100 \times 6 = 600$ for this study. The fitness (error) function tolerance was chosen to be $1e^{-4}$.

19.3 Results and Discussion

19.3.1 Sensitivity Analysis

Table 19.2 shows the result of sensitivity analysis carried out using Taguchi-based design of experiments. The data of 27 experiments carried out according to L_{27} orthogonal array was used to get information about the sensitivity of output towards individual parameters.

Table 19.2 Analysis of Variance (ANOVA) for different parameters

Source	DF	Adj SS	Adj MS	F-Value	% Contribution
E	2	5597,885,401	2798,942,700	3630.33	11.20
C_s	2	16,004,929,654	8002,464,827	10,379.48	32.01
m_s	2	22,166,899,947	11,083,449,973	14,375.63	44.34
C_t	2	6207,522,908	3103,761,454	4025.69	12.42
m_t	2	14,961,103	7480,552	9.70	0.03
t_ε	2	92,652	46,326	0.06	0.00
Error	14	10,793,843	770,989		
Total	26	50,003,085,508			

The '% Contribution' data, which is a measure of variation contributed by individual parameters towards the output, shows that except for t_ε all other parameters contributed towards the overall variation of output. However, the contribution was significantly influenced by the 'steady state' parameters (C_s and m_s).

19.3.2 Surrogate Model Training and Inverse Analysis

The findings from the sensitivity analysis was taken into account to revise the number of levels for each nonlinear Burgers model parameter. As discussed, t_ε showed no influence over the output of the nanoindentation simulations. Thus, in order to reduce computational expense, t_ε was given a constant value.

The two parameters that were the most influential of the remaining five, C_s and m_s, were varied at four levels. Meanwhile, moderately influential two parameters, E and C_t, were varied at three levels, while m_t was varied in two levels.

Table 19.3 shows the corresponding levels for each parameters that were selected based on the sensitivity analysis. In a full factorial basis, a total of $3 \times 4 \times 4 \times 3 \times 2 \times 1 = 288$ finite element simulations were carried out in order to generate the surrogate model for every single experimental conditions. In each of these simulations, 100 load–displacement data points were used to represent the nanoindentation plot. Since there were four individual experimental conditions to represent, a total of four surrogate models were developed. The snapshot matrix used to generate each of these surrogate model had dimensions of 100×288.

After the POD model reduction process was carried out and the RBF coefficients were calculated, the POD–RBF surrogate model was ready to approximate nanoindentation data within the specified parametric space (Table 19.1). An objective function was written in MATLAB where each surrogate model's output was compared against the corresponding experimental data. This objective function was used within the MATLAB Global Optimization Toolbox to run multi-objective genetic algorithm-based global optimization. The optimization algorithm was set to run in parallel mode until it met the stopping criteria. Table 19.4 shows the result from the global optimization algorithm.

The optimized set of parameters were the numerical best fits depending on the objective function that produces the numerical difference between the predicted and experimental data. Figure 19.2 shows the comparison of predicted and experimental data for all four experimental cases. These were the experimental conditions that were closely followed in creating finite element models and were used to train the predictive or surrogate model. From Fig. 19.2 it can be seen that all four surrogate model outputs were very close to the corresponding experimental data. This demonstrated the fact that the multi-objective genetic algorithm-based optimization procedure was successful in finding a common minima taking the constraints in to consideration.

Although, the surrogate model prediction's were mostly close with the experimental data few inconsistencies were observed. For example, the final unloading portion data for the loading–unloading time $t = 30$ s did not match very well. Similar behavior was observed for $t = 45$ s, even though qualitatively the difference between prediction and experiment diminished. For higher loading–unloading time, e.g. $t = 60$ s and 240 s, the difference was noticeably very small.

Table 19.5 shows quantitative variation between the various plots in Fig. 19.2. Variations between the plots has been represented in terms of RMSE, R^2, Avg. Error, and % Error. As it can be seen, quantitative discrepancies for different plots

Table 19.3 Parametric space of nonlinear Burgers parameters for surrogate training

Parameters	No of points in space	Parametric value space
E	3	3, 3.25, 3.5
C_s	4	0.02, 0.045, 0.07, 0.1
m_s	4	0.35
C_t	3	0.15, 0.25, 0.35
m_t	2	0.2, 0.8
t_ε	1	0.25

Table 19.4 Optimized nonlinear Burgers model parameters

Parameters	E	ν	C_s	m_s	C_t	m_t	t_ε
Optimized	3.28	0.34	0.09	0.20	0.24	0.47	0.25

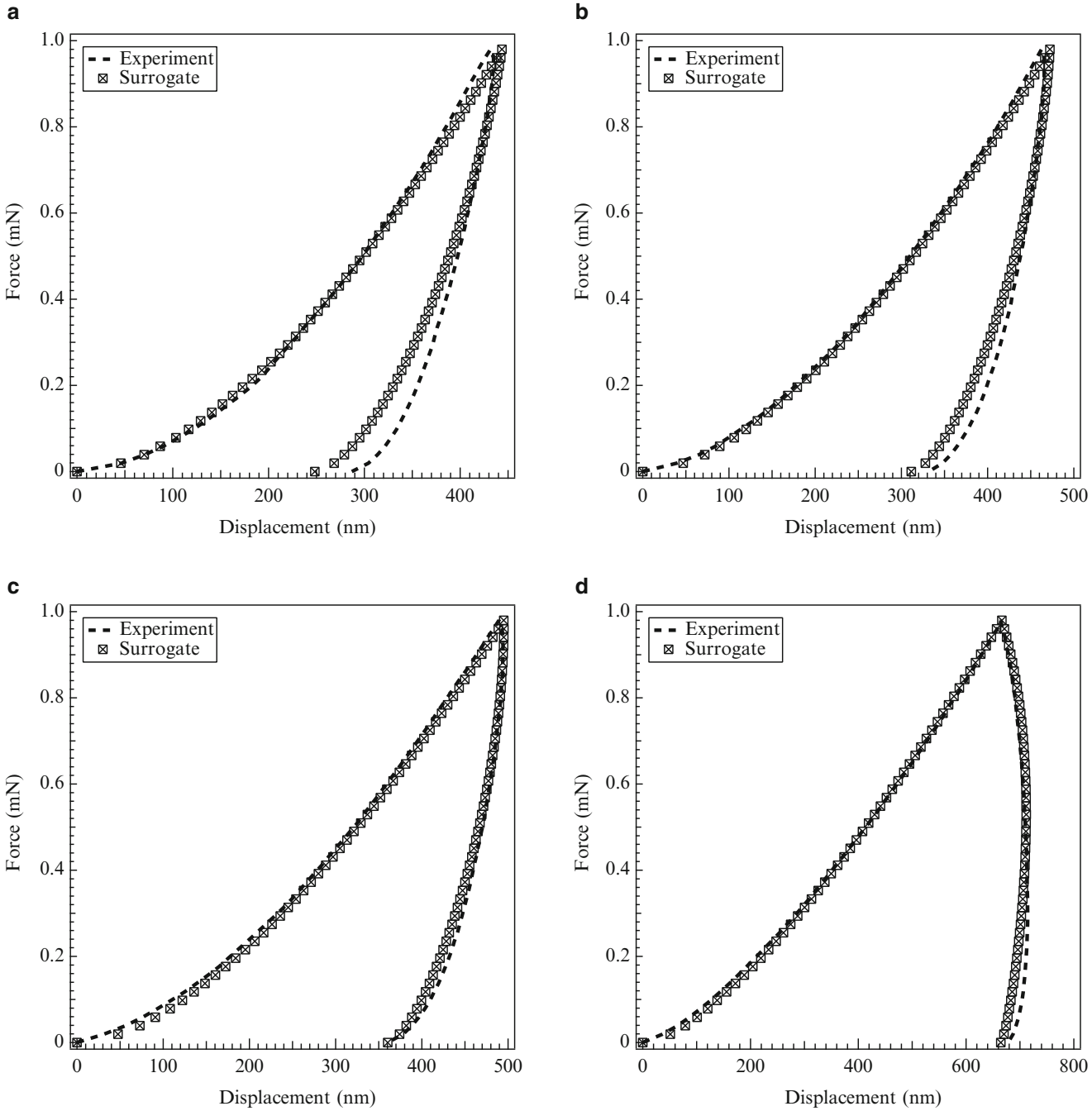

Fig. 19.2 Experiment vs. surrogate model for calibrated nonlinear Burgers model parameters. (**a**) Loading–unloading time = 30 s, (**b**) loading–unloading time = 45 s, (**c**) loading–unloading time = 60 s, (**d**) loading–unloading time = 240 s

Table 19.5 Variation between different plots

Conditions		RMSE	R^2	Avg. Err. (nm)	% Error
P_{max} = 1. 0 mN	t = 30 s	13.23	0.9821	9.11	2.81
	t = 45 s	9.17	0.9867	7.11	2.34
	t = 60 s	6.72	0.9891	5.70	2.81
	t = 240 s	9.01	0.9893	7.07	2.33

P_{max} = maximum load, t = loading–unloading time

of Fig. 19.2 were found to be comparable with each other. Another observation that could be made was that Fig. 19.2b and d both showed almost same quantitative variation. Although, Fig. 19.2d's match looked slightly better than Fig. 19.2b if perceived visually.

19.4 Conclusion

In this study, the model parameters for a nonlinear viscoelastic model has been identified using finite element based inverse analysis. A genetic algorithm-based optimization procedure was utilized where the load–displacement data was approximated using a surrogate model. A sensitivity analysis based on Taguchi method and ANOVA analysis was carried out to reduce the number of training points for the surrogate model. The POD–RBF based surrogate model was capable of producing good approximation for the nanoindentation experiment. The identified parameter set produced good match between experimental and surrogate-based load–displacement data.

Ascertaining that the material model parameter set that has been extracted from the inverse analysis procedure is indeed the global parameter set that would satisfy all possible material response is a challenge. In order to deal with this challenge, material responses from other experiments, such as compression, tension, or flexural tests could be included in the process. For some materials carrying out the aforementioned tests may not be feasible, e.g. thin films, coatings, biological cells. In those cases improving the confidence in the optimized parameter set could be established by obtaining material response data from multiple nanoindentation experiments, such as changing the cone angle for a pyramidal indenter tip, or using spherical tips with different radii.

Another way of finding additional constraints for the numerical analysis would be use additional experimental data from the same nanoindentation experiment. For example, if imprint geometry or residual depth profile data could be harnessed from a nanoindentation experiment and used in the objective function, the probability of finding the unique model parameter set increases.

An investigation is currently ongoing to validate the identified parameter set for different experimental conditions.

Acknowledgements We gratefully acknowledge that this work is funded in part or fully by a grant through the Oklahoma Nanotechnology Applications Project (ONAP) (Grant no. O9-20) and NASA Experimental Program to Stimulate Competitive Research (EPSCOR) (Grant no. NNXO9AP68A).

References

1. Hamim, S.U.A.: Variation of mechanical properties due to hygrothermal ageing and permanent changes upon redrying in clay/epoxy nanocomposites. ProQuest Dissertations and Theses, p. 49 (2011)
2. Hamim, S.U., Singh, R.P.: Effect of hygrothermal aging on the mechanical properties of fluorinated and nonfluorinated clay-epoxy nanocomposites. Int. Sch. Res. Not. **2014**, 1–13 (2014)
3. McKee, C., Last, J., Russell, P., Murphy, C.: Indentation versus tensile measurements of Young's modulus for soft biological tissues. Tissue Eng. B Rev. **17**(3), 155–164 (2011)
4. Hamim, S.U., Mishra, K., Singh, R.P.: Effect of UV exposure on mechanical properties of POSS reinforced epoxy nanocomposites. In: 2014 Annual Conference on Experimental and Applied Mechanics (2014)
5. Zhang, J., Michalenko, M.M., Kuhl, E., Ovaert, T.C.: Characterization of indentation response and stiffness reduction of bone using a continuum damage model. J. Mech. Behav. Biomed. Mater. **3**(2), 189–202 (2010)
6. Engels, P., Begau, C., Gupta, S., Schmaling, B., Ma, A., Hartmaier, A.: Multiscale modeling of nanoindentation: from atomistic to continuum models. Nanomechanical Analysis of High Performance Materials, pp. 285–322. Springer, Netherlands (2013)
7. Doerner, M., Nix, W.: A method for interpreting the data from depth-sensing indentation instruments. J. Mater. Res. **1**(04), 601–609 (1986)
8. Oliver, W., Pharr, G.: An improved technique for determining hardness and elastic modulus using load and displacement sensing indentation experiments. J. Mater. Res. **7**, 1564–1583 (1992)
9. Li, X., Bhushan, B.: A review of nanoindentation continuous stiffness measurement technique and its applications. Mater. Charact. **48**(1), 11–36 (2002)
10. Fischer-Cripps, A.: Nanoindentation. Springer, New York (2004)
11. Ngan, A.: Nanomechanical characterization of soft materials. In: Tiwari, A. (ed.) Nanomechanical Analysis of High Performance Materials. Springer, Netherlands (2014)
12. Marin, J., Pao, Y.: An analytical theory of the creep deformation of materials. J. Appl. Mech. **20**, 245–252 (1953)
13. Richter, H., Misawa, E., Lucca, D., Lu, H.: Modeling nonlinear behavior in a piezoelectric actuator. Precis. Eng. **25**(2), 128–137 (2001)
14. Shames, I., Cozzarelli, F.: Elastic and Inelastic Stress Analysis. Taylor and Francis, Washington (1997)

15. Kucuk, Y.: Simulation of non-linear viscoelastic behavior of cross-linked mesoporous silica aerogels by depth-sensing indentation. Indian J. Eng. Mater. Sci. **19**(4), 260–268 (2012)
16. Kucuk, Y., Mollamahmutoglu, C., Wang, Y., Lu, H.: nonlinearly viscoelastic nanoindentation of PMMA under a spherical tip. Exp. Mech. **53** (5), 731–742 (2012)
17. Hamim, S.U., Singh, R.P.: Taguchi-based design of experiments in training POD-RBF surrogate model for inverse material modeling using nanoindentation. Inverse Prob. Sci. Eng. (2016). doi:0.1080/17415977.2016.1161036
18. Magnenet, V., Giraud, A., Homand, F.: Parameter sensitivity analysis for a Drücker–Prager model following from numerical simulations of indentation tests. Comput. Mater. Sci. **44**(2), 385–391 (2008)
19. Ma, Y., Zhang, Y., Yu, H.-F., Zhang, X.-Y., Shu, X.-F., Tang, B.: Plastic characterization of metals by combining nanoindentation test and finite element simulation. Trans. Nonferrous Metals Soc. China **23**(8), 2368–2373 (2013)
20. Clément, P., Meille, S., Chevalier, J., Olagnon, C.: Mechanical characterization of highly porous inorganic solids materials by instrumented micro-indentation. Acta Mater. **61**(18), 6649–6660 (2013)
21. Chatterjee, A.: An introduction to the proper orthogonal decomposition. Curr. Sci. **78**(7), 808–817 (2000)
22. Liang, Y.C., Lee, H.P., Lim, S.P., Lin, W.Z., Lee, K.H., Wu, C.G.: Proper orthogonal decomposition and its applications - Part I: theory. J. Sound Vib. **252**(3), 527–544 (2002)
23. Ly, H., Tran, H.: Modeling and control of physical processes using proper orthogonal decomposition. Math. Comput. Model. **33**(1–3), 223–236 (2001)
24. Buljak, V.: Inverse Analyses with Model Reduction. Computational Fluid and Solid Mechanics. Springer, Berlin/Heidelberg (2012)
25. Rogers, C., Kassab, A., Divo, E., Ostrowski, Z., Bialecki, R.: An inverse pod-rbf network approach to parameter estimation in mechanics. Inverse Prob. Sci. Eng. **20**, 749–767 (2012)